

# Model of energetic electron transport in magnetron discharges

T. E. Sheridan, M. J. Goeckner, and J. Goree

*Department of Physics and Astronomy, The University of Iowa, Iowa City, Iowa 52242-1410*

(Received 12 June 1989; accepted 5 August 1989)

A particle model of energetic electron transport in sputtering magnetron discharges is presented. The model assumes time-independent magnetic and electric fields and supposes that scattering by neutral atoms is the dominant transport mechanism. Without scattering, we find that some orbits are confined indefinitely. Using the differential cross sections for elastic, excitation, and ionization collisions in argon, we perform a Monte Carlo simulation of the electrons emitted by ion bombardment of a planar magnetron cathode to predict the spatial distribution of ionization. We find good agreement with experimental measurements of the radial profile of ion flux to the cathode and of the axial profile of optical emission.

## I. INTRODUCTION

Magnetrons are magnetized plasma devices that are widely used as sputtering sources for thin film deposition. There are several geometrical configurations, including cylindrical magnetrons,<sup>1</sup> planar magnetrons,<sup>2</sup> and sputter guns.<sup>3</sup> All of them rely on a cathode that is bombarded by ions to produce the desired sputtering flux.

In addition to sputtering, the ion bombardment is responsible for secondary electron emission at the cathode. The resulting electrons are accelerated by an electric field and gain an energy equivalent to the cathode bias, which is typically 300–500 eV.

Magnetrons are all characterized by nonuniform electric and magnetic fields  $\mathbf{E}$  and  $\mathbf{B}$  that are configured to provide confinement of electrons in the vicinity of the cathode. The electric field is established by the electric sheath between the plasma and the cathode,<sup>4</sup> while the magnetic field is provided externally by a set of permanent magnets or electromagnets located behind the cathode. In all types of magnetrons, the electrons are confined in a closed circuit in which they move in the  $\mathbf{E} \times \mathbf{B}$  direction. As a result of confining the electrons near the cathode, it is possible to operate the discharge at a lower neutral pressure and a lower discharge voltage than would be required without confinement.

An adequate picture of the confinement mechanism has been introduced by Wendt *et al.*<sup>5</sup> It is based on the Hamiltonian mechanics formalism of the effective potential energy surface, which we will review in Sec. II.

However, an adequate model has not yet been reported for electron transport. Such a model must attribute the scattering of electrons out of the region of confinement to some mechanism. Some candidate scattering mechanisms are collisions with neutrals, Coulomb collisions with ions, and collective effects such as turbulent transport.

Other researchers proposed that turbulence is responsible for electron transport.<sup>6</sup> Low-frequency turbulence is characterized by random electric fields that result in random  $\mathbf{E} \times \mathbf{B}$  velocities, which perturb an electron out of its stable orbit. In Ref. 7, a measurement of the turbulence level and the confinement time  $\tau$  was described, which showed that low-frequency turbulent transport is negligible for low energy electrons. For energetic electrons, it is likely that the random

$\mathbf{E} \times \mathbf{B}$  velocities would be the same, and that their turbulent transport would also be negligible. Consequently, another transport mechanism must be found and tested. One possibility is high-frequency turbulence; another is collisions. Here, we propose that collisions with neutrals account for the transport of energetic electrons.

Throughout this paper, we will refer to two categories of electrons, fast and bulk, according to their origin. Fast electrons originate at the cathode or in the sheath, while the bulk electrons are created in the main discharge region. We also introduce the term *energetic*, which refers to those electrons that have enough energy to ionize neutrals. This designation includes all the fast electrons as well as the tail of the bulk distribution. The model developed here is applicable to the energetic electrons.

Section II describes electron and ion orbits in the absence of collisions. In contrast to the electrons, we find that the ions are not magnetized, i.e., their orbits are not deflected significantly by the magnetic field. Section III introduces elastic, excitation, and ionization electron collisions. The assumptions of our model, which is applicable to all magnetron geometries, are described in greater detail there. For the planar magnetron geometry, in particular, we have developed a Monte Carlo code implementation of the model, which is described in Sec. IV. All the energetic electrons can be treated using this method, although in this paper we concentrate on applying it to the fast electrons that are emitted from the cathode. Section V presents simulation results, where we find good agreement with experimental data.

## II. COLLISIONLESS SINGLE PARTICLE ORBITS

Here we will consider the orbits of single particles, both electrons and ions, in the magnetron geometry. In this picture, the particles respond to prescribed electric and magnetic fields. Because this is a single-particle model, self-consistent plasma behavior resulting in changes in the fields is neglected.

This section will establish that some electrons are confined. We will first introduce the concept of the effective potential and then present some illustrations of typical particle orbits. We will consider only collisionless orbits. Of

course the particles actually do undergo collisions, which we will treat in Sec. III.

### A. Effective potential

Two approaches to understanding the motion of an electron in given electric and magnetic fields are the use of the equation of motion

$$\ddot{\mathbf{x}} = \frac{q}{m}(\mathbf{E} + \mathbf{v} \times \mathbf{B}) \quad (1)$$

and the Hamiltonian mechanics picture.<sup>8</sup> Wendt *et al.*<sup>5</sup> presented the Hamiltonian approach as a helpful conceptual way of understanding the particle motion in a magnetron. In this formalism, the electron moves about on an effective surface in much the same way that a marble rolls in a bowl. The shape of the bowl determines the region that is energetically accessible to the marble, and it will confine the marble if its surface is high enough all around. Similarly, the effective potential surface of the magnetron can confine an electron.

Consider the case of a planar magnetron that is cylindrically symmetric, as shown in Fig. 1. The effective potential  $\Psi$  is independent of the azimuthal coordinate  $\theta$ . Adopting a cylindrical coordinate system  $(r, \theta, z)$ , where  $z$  is the axial coordinate measured from the cathode surface, the canonical momentum

$$P_\theta = mr^2\dot{\theta} + qA_\theta r \quad (2)$$

is conserved as the electron moves about. Here,  $A_\theta$  is the magnetic vector potential, which depends on  $r$  and  $z$ . The effective potential energy is then

$$\Psi = \frac{(P_\theta - qA_\theta r)^2}{2mr^2} + q\phi, \quad (3)$$

where  $q$  is the charge and  $\phi$  is the electric potential. Note that  $\Psi$  has both a magnetic component (the first term) and an electric component (the second term). Since it does not de-

pend on  $\theta$ , the effective potential energy is two-dimensional,  $\Psi = \Psi(r, z)$ . For each electron with a different  $P_\theta$ , the effective potential  $\Psi(r, z)$  is different.

The  $z$  dependence of the shape of  $\Psi$  is sketched in Fig. 2. In the sheath region of the discharge, the electric part  $q\phi$  repels electrons from the cathode. For larger values of  $z$ , the magnetic component of  $\Psi$  rises, preventing electrons from moving far away from the cathode. (While the magnetic part depends on  $P_\theta$ , the electric part  $q\phi$  does not.) The sum of the electric and magnetic parts of  $\Psi$  forms a trap, as shown by the curve for total effective potential.

The shape of  $\Psi$ , shown in Fig. 2, is only a sketch of the  $z$  dependence. To find the exact two-dimensional effective potential surface, we must use specific forms for the electric and magnetic components, i.e., we must specify  $\phi$  and  $A_\theta$ . For  $A_\theta$ , we will use the magnetic configuration of the cylindrically symmetric planar magnetron described in Ref. 7, which has a magnetic field with a purely radial component of 245 G at  $r = 1.7$  cm on the cathode surface. The computed field was calibrated against experimental measurements.

We assume that  $\phi$  depends only on  $z$ , and consists of a sheath and a presheath. For the sheath portion, we use the improved Child's law expression developed in Ref. 9. [This model for  $\phi(z)$  is appropriate for sheaths that are collisionless and source-free. Since those two requirements are not strictly met in magnetrons, the use of this model here is an approximation.] The sheath is connected smoothly to a presheath with a uniform electric field of 1 V/cm, a value which was chosen to provide a potential drop of  $kT_e/q$  over an interval of 4 cm. Here,  $k$  is Boltzmann's constant and  $T_e$  is the electron temperature.

Contour plots of  $\Psi(r, z)$  are presented in Fig. 3 for two different values of  $P_\theta$ . (By selecting an initial radius and

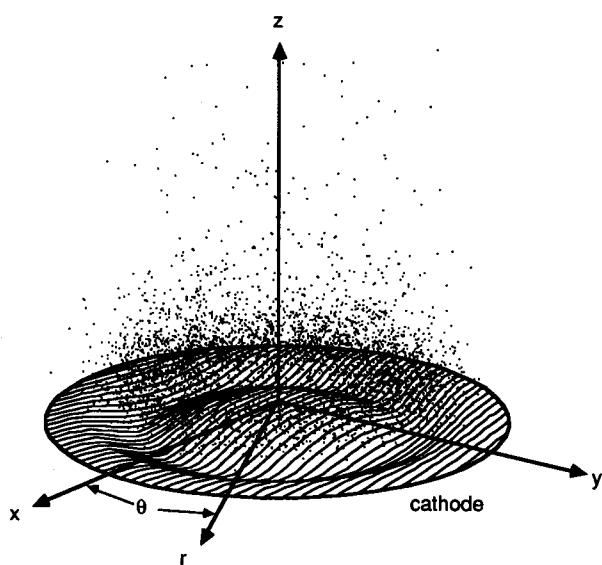


FIG. 1. Planar magnetron. The disk-shaped cathode surface shows an etch track formed by ion bombardment sputtering. A representation of the ionization distribution, prepared using the simulation described in this paper, is shown by the dots. The coordinate systems used are indicated.

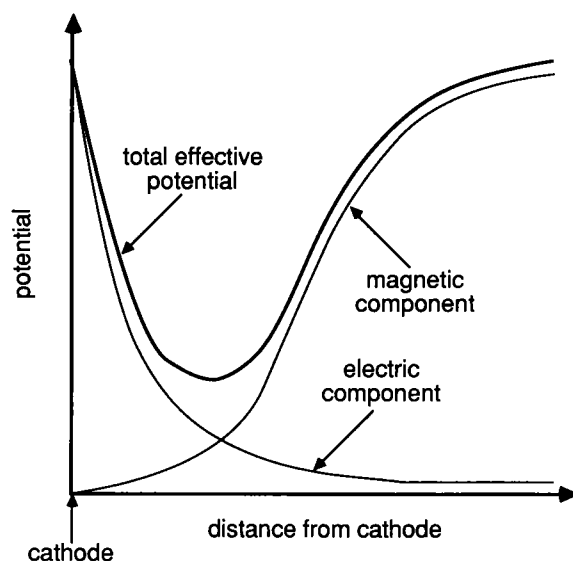


FIG. 2. Sketch of the effective potential  $\Psi$  for an electron. The electric component of the potential appears mainly in the sheath region near the cathode. It accelerates electrons away from the cathode, giving them energy as they move into the plasma region, and it keeps electrons in the plasma from escaping to the cathode. The magnetic component keeps electrons from escaping from the vicinity of the cathode surface. This combination results in a potential well where some electrons are confined.

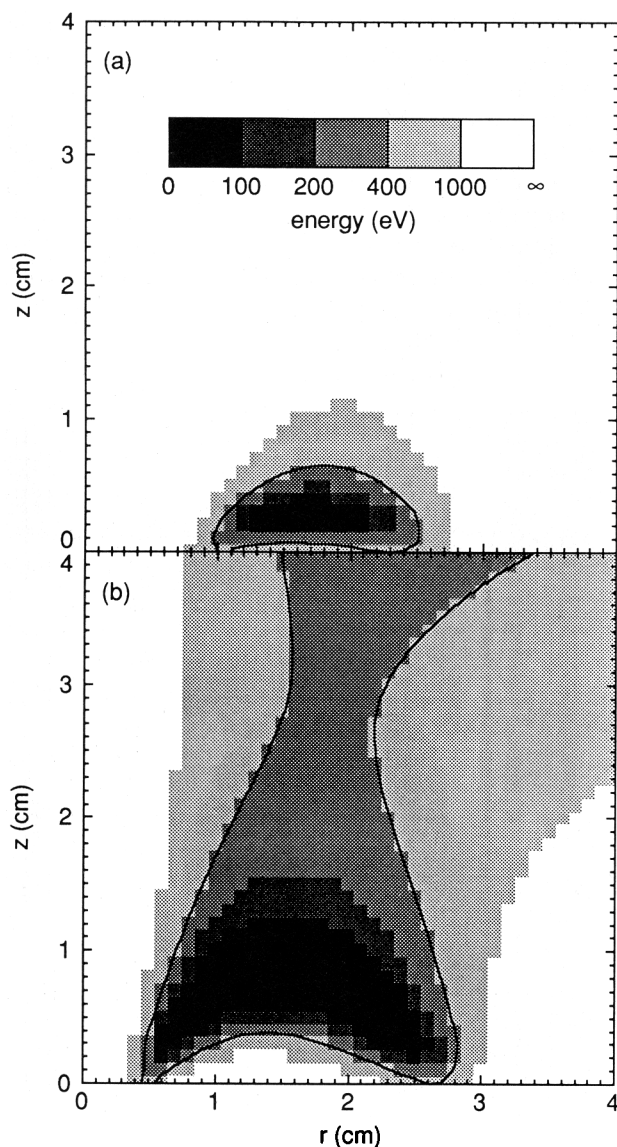


FIG. 3. Plot of the effective potential surface  $\Psi(r,z)$  for an electron born with zero velocity on the cathode ( $z = 0$ ), computed for the planar magnetron described in Ref. 8, with a 400 V bias on the cathode. The unit of energy is eV, as shown in the bar scale. The potentials shown were computed for the following values of the canonical momentum  $P_\theta$ : (a)  $3.51 \times 10^{-25} \text{ kg m}^2/\text{s}$ , corresponding to a starting radius  $r_i = 1.0 \text{ cm}$ , and (b)  $1.14 \times 10^{-25} \text{ kg m}^2/\text{s}$ , corresponding to  $r_i = 0.5 \text{ cm}$ . The contour shown with a heavy line bounds the region accessible to an electron of total energy 400 eV. In (a) an electron is confined indefinitely in the absence of scattering, while in (b) it can escape out the top.

setting the initial velocity to zero,  $P_\theta$  is determined.) The region inside the heavy contour is accessible to an electron if the cathode is biased at 400 V. For the starting radius selected in Fig. 3(a), a 400 eV electron will never leave the trap as long as there is no scattering event to change  $P_\theta$ . This is what is meant by the term confinement. In Fig. 3(b), on the other hand, electrons emitted at the same electric potential can escape through the open end at the top of the figure.

In examining these contours, one must remember that they are plots of the effective potential energy  $\Psi$  as a function of only two spatial coordinates,  $r$  and  $z$ , since it does not depend on  $\theta$ . While this surface is two dimensional, the mo-

tion of an electron is, of course, still three dimensional. The electron revolves around the  $z$  axis, and this azimuthal rotation is superimposed on the motion in the two-dimensional potential well.

## B. Orbits

Using the magnetic and electric fields from the models described above, and integrating the equation of motion [Eq. (1)] in three dimensions, by using a fourth-order Runge-Kutta routine,<sup>10</sup> we produced plots of the electron and ion orbits.

Orbits are shown in Fig. 4 for an electron that was released from the cathode with zero velocity at the same starting radii as in Fig. 3. In the  $r$ - $z$  projection of Fig. 4(a), the electron moves about in a confined region determined by the kidney-shaped potential well. In Fig. 4(b), the same orbit is shown projected on the cathode, i.e., the  $x$ - $z$  plane. It has a starfish shape resulting from the combination of azimuthal rotation and bouncing in the potential well. This collisionless orbit is confined indefinitely. In contrast, the orbit displayed in Figs. 4(c) and 4(d) is unconfined. This particle is lost through the open end of the  $\Psi(r,z)$  surface of Fig. 3(b).

When an electron begins at  $r = 1.7 \text{ cm}$ , which is known from experiments to be near the center of the plasma cross section, the orbit remains on a single surface of rotation, and takes on a cycloidal shape. The cycloid is, however, a unique case; most trapped orbits resemble the one shown in Figs. 4(a) and 4(b).

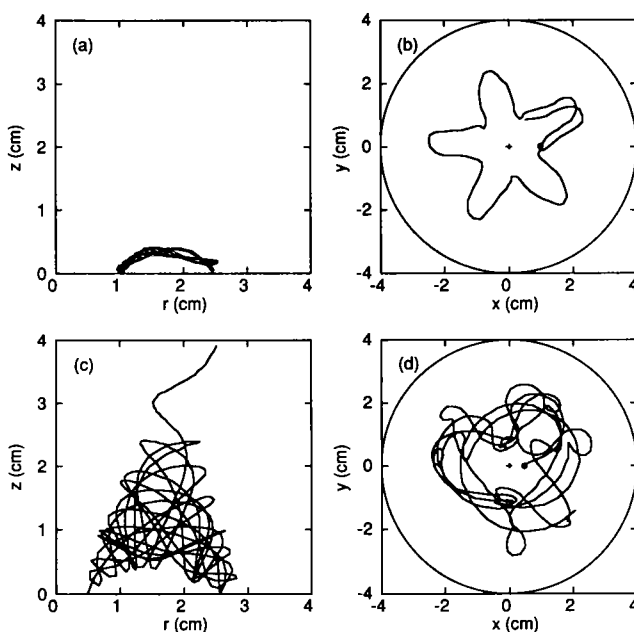


FIG. 4. Orbits for an electron born on the surface of the cathode. The orbit began at rest at the dot located at  $z = 0 \text{ cm}$  and  $r = 1.0 \text{ cm}$  in (a) and (b), corresponding to the effective potential shown in Fig. 3(a). Here, (a) is a projection of the orbit onto the  $r$ - $z$  plane, and (b) is a projection onto the  $x$ - $y$  plane, that is, the cathode surface. This collisionless orbit is confined indefinitely. For (c) and (d), the orbit began at  $r = 0.5 \text{ cm}$ , corresponding to Fig. 3(b). This unconfined orbit escapes after several bounces. (These diagrams were made by integrating the equation of motion with a time step of 50 ps, and connecting the points recorded at every fourth time step.)

In all cases, the paths of *energetic* electrons do not have the helical shape characteristic of Larmor orbits. This is a consequence of the gyroradius being comparable to the scale length of the magnetic field. The orbits revolve around the  $z$  axis in the  $\mathbf{E} \times \mathbf{B}$  direction.

Ion trajectories computed for the planar magnetron device are shown in Fig. 5. They differ markedly from the orbits of electrons as a consequence of their higher mass. In effect, the ions are not magnetized. They fall directly to the cathode with very little radial displacement. This observation is used in the physical model of energetic electron transport that we develop next.

### III. TRANSPORT MODEL

In Sec. II we showed that there are electron orbits that are confined indefinitely in a trap in the absence of some scattering mechanism. This serves as motivation for the need to model transport. In this section, we will describe a physical model in which the energetic electrons are scattered by collisions with neutrals.

#### A. Assumptions

Our model portrays single electrons as if they respond to prescribed, time-independent  $\mathbf{E}$  and  $\mathbf{B}$  fields and suffer collisions at random intervals. Collective plasma effects, which would alter the fields and change an electron's energy, are neglected. The ions are treated as if they are unmagnetized. They fall directly from their point of origin toward the cathode; assuming a one-dimensional electric field, they fall without any radial deflection. When they strike the cathode, the ions create secondary electrons that initially have a kinetic energy of typically 1–4 eV,<sup>11</sup> which we approximate to be zero.

Initially, two types of electron collisions, with neutrals and with ions, must be evaluated. Consider a typical magnetron discharge having an ion density of  $2 \times 10^{10} \text{ cm}^{-3}$  and room temperature argon at a pressure of 1 Pa. For a 400 eV electron, the perpendicular momentum deflection collision frequency is 14 MHz for scattering by neutrals, but only 250 Hz for scattering by ions. Accordingly, we neglect Coulomb collisions in our magnetron model.

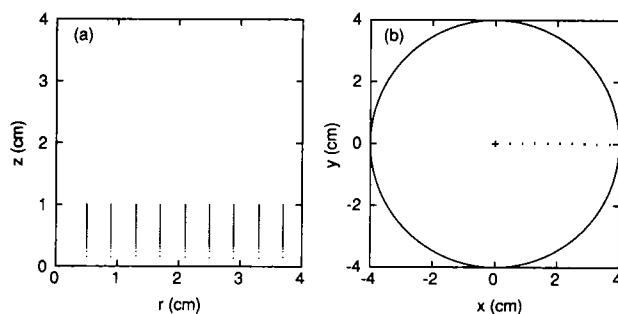


FIG. 5. Orbits of ions born at  $z = 1 \text{ cm}$ . The paths followed by  $\text{Ar}^+$  are shown for several initial radii. The ions are released at  $z = 1 \text{ cm}$  with zero initial velocity, and then the presheath electric field accelerates them to the surface of the cathode. As they fall, they are deflected slightly in the azimuthal direction, but only a negligible amount in the radial direction. The electric potential is assumed here to vary with  $z$  but not  $r$ .

#### B. Neutral collisions

The history of a fast electron can be summarized as follows. After it is created on the cathode or in the sheath, it falls down the potential hill of the sheath, gaining energy. It slowly loses this energy due to collisions with neutrals. Meanwhile, the orbit swirls about in the potential well, and it may or may not be trapped. Every time a collision takes place, an electron that is trapped may be scattered into an unconfined orbit and become lost from the system. Thus, some fast electrons will be confined long enough to perform a large number of ionizations, while others will be present only long enough to perform a few or even none at all. As a result of all these ionizations, the bulk electron population is formed.

In our treatment, three types of collisions with neutrals are taken into account: elastic scattering, ionization, and excitation. All these collisions result in scattering the direction of the electron's velocity and reducing its energy. However, several collision processes are neglected. We do not allow for the possibility of a single collision resulting in either a double ionization (which accounts for 6% of the total inelastic cross section at  $E = 100 \text{ eV}$ ), nor do we allow the production of an excited state of an ion (which accounts for less than 1% of the total).<sup>12</sup> Additionally, Penning ionization and two-step ionization are not accounted for.

The energy lost in a collision depends on its type. Ionizing events result in the greatest energy loss, which is the ionization potential (15.8 eV for ground state argon) plus the kinetic energy of the newly released electron. The energy lost in an excitation collision (11.6–15.8 eV for argon) depends on the energy level to which the neutral is excited. Of the three types of collisions, an elastic scattering consumes the least energy. The fractional loss is on the order of the mass ratio,  $\Delta K/K = (4m_e/M) \sin^2(\alpha/2)$ , where  $m_e$  and  $K$  are the mass and kinetic energy of the electron,  $M$  is the mass of the neutral, and  $\alpha$  is the angle by which the velocity is deflected.

All three types of collisions are characterized by a differential scattering cross section  $d\sigma/d\Omega$  that predicts the probability per unit solid angle of scattering into an angle  $\alpha$  for a given energy  $K$ . For ionization collisions in particular, a full differential cross section would also be specified as a function of the energy of the newly created electron.<sup>13</sup>

The angular dependence of the differential cross section  $d\sigma/d\Omega$  varies with energy. For most gases, the cross sections are nearly isotropic for low electron energies, while for  $K > 60 \text{ eV}$  they are generally peaked for small values of  $\alpha$ , i.e., for forward scattering.

This predominance of forward scattering means that  $P_\theta$  and consequently  $\Psi$  are not changed greatly in most collisions. Hence, an electron may suffer many collisions before it is scattered out of a confining well. If the confinement is effective, energetic electrons may use up almost all of their energy before they are lost, thereby maximizing the ion production.

### IV. NUMERICAL IMPLEMENTATION

In the physical model described above, electrons move in prescribed electric and magnetic fields, subject to collisions

at random intervals. This type of model is well suited for application in a Monte Carlo computer code. Using such a code involves following the orbits of a large number of electrons one at a time; keeping track of their location, velocity, and kinetic energy; and allowing them to scatter in collisions. To do this, we must provide expressions for the electric and magnetic fields, push the electrons with an integrator based on the equation of motion, and provide accurate differential scattering cross sections. Additionally, the use of Monte Carlo codes requires that initial conditions for each particle be chosen in an unbiased fashion to obtain meaningful results.

We have implemented our physical model with a fully three-dimensional Monte Carlo program. In this section, we describe its operation and list the approximations that it entails.

### A. Integrating the orbits

The equation of motion to be integrated is Eq. (1). It is integrated in single steps according to a fixed time step  $\Delta t$  by using the same fourth-order Runge-Kutta method as in Sec. II. To follow the orbit accurately, the value of  $\Delta t$  is chosen to be small compared to both the gyroperiod and the inverse collision frequency and to provide energy conservation.

The electric and magnetic fields used here are the same as those described in Sec. II. The magnetic field is recorded in a two-dimensional grid in the  $r$ - $z$  plane, while the electric field is gridded in one coordinate  $z$ . Interpolation is used to evaluate the fields between grid points.

### B. Collisions

At each time step during an electron orbit, we determine whether a collision has taken place. This is done by generating a random number that is compared to the probability per unit time of a collision. For argon, we use the total cross sections reported in Refs. 14 and 15, and interpolate between tabulated values.

When it has been determined that a collision takes place, another random number is generated to determine whether it was an elastic, excitation, or ionization event. This is evaluated according to the relative cross sections of these processes.

According to the type of collision, the energy of the energetic electron is reduced. In our current code we approximate that the energy lost in an excitation or ionizing collision is always a fixed amount, 11.6 eV for excitation and 15.8 eV for ionization of argon. By using a fixed energy loss for ionization, we ignore the kinetic energy of the secondary electron released in an ionization event. That energy is almost always much smaller than the energy of the ionizing electron.<sup>13</sup> Accordingly, we use a reduced scattering cross section for ionization that does not depend on the energy of the secondary electron.

In addition to decrementing the energy of the energetic electron when it undergoes a collision, we randomly scatter its velocity into a new direction, which is chosen in a manner consistent with the differential scattering cross section. For the energy range  $K < 3$  eV, we assume that the differential

cross sections are isotropic. For  $3 \text{ eV} < K < 3 \text{ keV}$ , we use the normalized values of  $d\sigma/d\Omega$  for elastic scattering that are tabulated in Ref. 16. We make the approximation that these are valid for all three types of collisions. The suitability of this simplification can be confirmed by an inspection of the shapes of  $d\sigma/d\Omega$  as a function of energy for the three types of collisions,<sup>13</sup> which reveals that they are nearly the same.

### C. Ensembles of orbits

An orbit must be terminated according to some criterion, such as: (1) it leaves the simulation region, (2) a fixed maximum time has elapsed, or (3) the energy is depleted below the level of the ionization potential. When this happens, a new energetic electron orbit is begun from a new initial position. This is repeated for an ensemble of electrons. After the last electron is finished, the user can produce useful results such as a spatial profile of ionization events.

The statistical quality of those results will be determined by both random and systematic errors. Random errors diminish according to the square root of the number of electrons in the ensemble. The larger the ensemble size, the smaller the random errors will be. Of course the computer time required increases linearly with the number of electrons, so the user cannot choose the ensemble size to be arbitrarily large but rather chooses it to give the size of error bars desired.

On the other hand, systematic errors are generally not improved upon by increasing the ensemble size. They must be eliminated by thoughtful planning of the code. One potential source of systematic errors that requires special attention in all Monte Carlo codes is the choice of the initial conditions for each electron.

### D. Initial conditions

Physically, the position at which each electron starts is different. Accordingly, in the numerical implementation, a different random starting position must be chosen for each electron. This must be done in a fashion that represents the physical processes involved. The code could be used with initial conditions chosen to simulate electrons born in the plasma and sheath regions, but in the present paper, we will treat only the electrons originating on the cathode due to ion bombardment.

The starting radius  $r_i$  for each electron is specified in the following convergent manner. The first electron is released from a random point. Subsequent electrons can originate from any point on the cathode, with some points more likely than others. To account for this, we use a radial probability profile  $P(r_i)$  to describe the probability per unit radius of an electron being born at  $r_i$ . Physically, each electron is responsible for ionizations that would result in ions falling directly down to the cathode, resulting in the emission of new electrons at the sites of ion impact. Accordingly, in the code,  $P(r_i)$  is updated according to the history of all previous ionizations before starting each new electron. This is done by counting the ionizations that took place in radial bins.

The probability profile converges to a recognizable steady state after about 30 fast electrons have been tracked. This

means that for many applications the code must be run for an ensemble of more than 30 electrons.

## V. RESULTS

As a test of the numerical implementation of our physical model, we ran an ensemble of 600 electrons originating at the cathode. The discharge was assumed to have the parameters of the experiment reported in Ref. 7: cathode bias of 400 V, argon gas pressure of 1 Pa,  $T_e = 4$  eV, and density appropriate to produce a Debye length of 0.1 mm. Under these conditions, the total collision mean free path is 1.7 cm for a 20 eV electron, and 9.4 cm for a 400 eV electron.

The time step  $\Delta t$  was selected to be 50 ps. This value was chosen to be small enough to provide 20 integration steps per gyroperiod in a 300 G magnetic field. It also provided at least 130 steps per collision, on average.

Orbits were followed until the electrons either escaped from the boundaries of our  $4 \times 4$  cm working space on the  $r$ - $z$  plane or until a limit of  $2.5 \mu\text{s}$  had elapsed, whichever came first. The time limit was chosen to be long enough that fewer than 0.5% of the remaining electrons had enough energy to result in an ionization. For this run, we did not stop orbits if the electron energy fell below the 15.8 eV ionization potential of argon.

### A. Collision statistics

We recorded the location and type of each collision. Defining the average number of ionizations per fast electron as  $\langle N_i \rangle$ , our run yielded  $\langle N_i \rangle = 14.26 \pm 0.44$ , where the uncertainty given is for a 90% confidence level. For comparison, consider that a 400 eV electron can produce at most  $N_{\text{max}} = 25$  ionizations, given the ionization potential of 15.8 eV for argon.

Note that if the discharge is to be maintained solely by ion bombardment of the cathode, then it is necessary that  $\langle N_i \rangle \geq \gamma^{-1}$ , where  $\gamma$  is the secondary electron emission coefficient. Since  $\gamma^{-1} \approx 10$  for many metals, our result that  $\langle N_i \rangle \approx 14$  confirms that cathode emission alone could sustain a magnetron plasma.

For the same ensemble of 600 fast electrons, there were an average of  $3.65 \pm 0.16$  excitation collisions per electron. This number is less than  $\langle N_i \rangle$  simply because the cross section for excitation is smaller than that for ionization.

The most frequent type of collision is elastic, because of its large cross section, especially for lower energies. Our ensemble experienced 48.67 elastic collisions per electron. Most of these occurred after the energy of a trapped electron had been depleted below the 11.6 eV excitation potential, where there is no possibility of inelastic collisions.

The distribution of the number of ionizing collisions per electron is shown in a histogram, Fig. 6. The most probable number of ionizations per fast electron was 20, which is at the center of a peak between 18 and 24 ionizations per electron. (The width of this peak is accounted for by excitation collisions.) Recalling the  $N_{\text{max}}$  is 25, we see that this peak indicates that many fast electrons remained trapped until most of their energy is lost. The other electrons performed a smaller number of ionizations and then escaped.

The confinement provided in an actual magnetron plasma

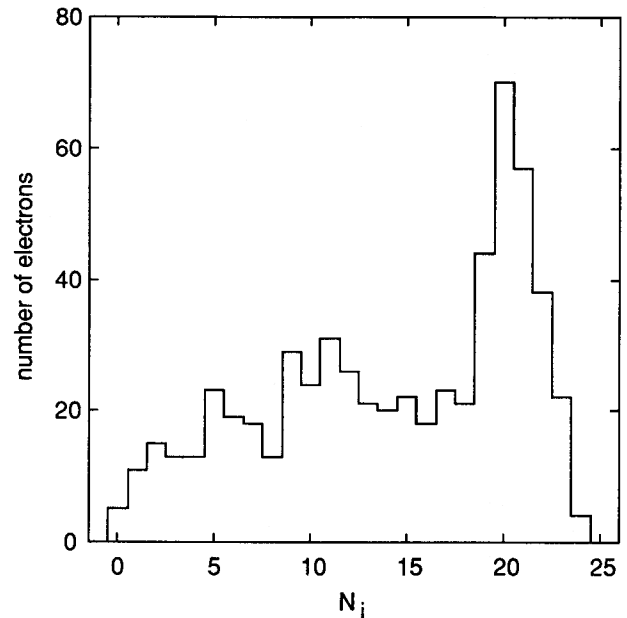


FIG. 6. Distribution of number of ionizing collisions for 600 electrons in argon at a pressure of 1 Pa. This histogram has a peak centered at 20 ionizations, which corresponds to electrons that lose all their energy in collisions without escaping from the trap. Elastic, excitation, and ionizing collisions are taken into account. The maximum possible number of ionizations is  $N_{\text{max}} = 25$ , which is the ratio of the 400 V cathode potential to the 15.8 eV ionization potential. The width of the peak is due to energy lost in excitation collisions.

works well, producing almost as many ionizations as possible. This is of course the advantage of the magnetron as a sputtering device.

The principal reason for the good confinement is the effective potential well. Furthermore, as we discussed at the end of Sec. III, most differential cross sections are peaked for forward scattering, which means that to scatter  $P_0$  enough to detrap the electron, many collisions may be required. To test this prediction, we performed a run for comparison where  $d\sigma/d\Omega$  was isotropic and found that  $\langle N_i \rangle$  was  $2.52 \pm 0.15$ , which is small compared to the value of 14.26 reported above. This indicates that in contrast to forward scattering, large angle scattering leads to a loss of confinement after fewer ionizations have occurred. Much of the magnetron's high ionization efficiency can thus be attributed to the predominance of forward scattering.

### B. Density of ionizing collisions

The density of ionization collisions  $\rho_i(r, z)$  is shown in Fig. 7. Recalling that the  $z$  axis is the axis of symmetry for the planar magnetron, an inspection of this illustration reveals that the ionization events are concentrated in a ring located above the cathode surface. Some of the ionization events from Fig. 7 were used to prepare Fig. 1, where the ring is shown in a three-dimensional view. The latter diagram bears a very close resemblance to the visual appearance of a planar magnetron discharge.

According to the physical model of electron transport, the ionization distribution is determined by electron orbits, which are determined by the shape of the effective potential

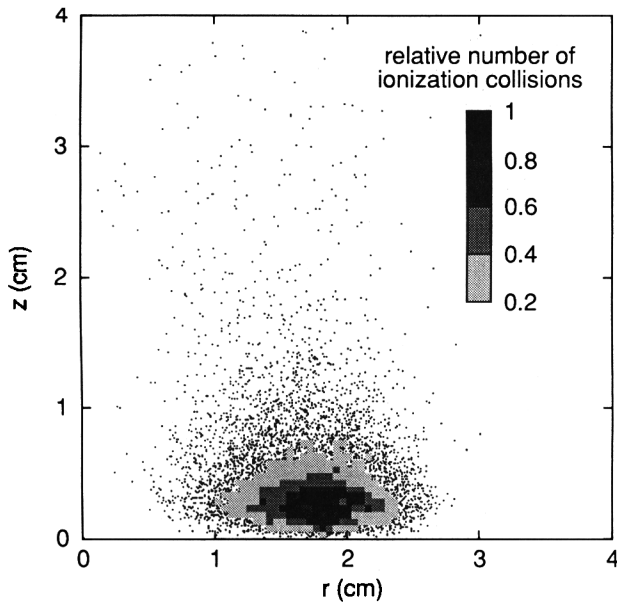


FIG. 7. Density of ionizing collisions,  $\rho_i(r, z)$ , plotted as a function of  $r$  and  $z$ . The locations of the ionization events were assigned to pixels  $0.5 \times 0.5$  mm in size to produce the gray-scale diagram. In pixels having less ionization than the bottom of the gray scale, the event locations are shown with dots. The region of strong ionization forms a ring separated from the cathode surface by a dark space. Note the similarity to the effective potential  $\Psi(r, z)$  shown in Fig. 3(b). The event locations indicated here were used in preparing the three-dimensional view in Fig. 1.

well. It is therefore instructive to compare  $\rho_i(r, z)$  in Fig. 7 to an effective potential well shape, such as Fig. 3. The shapes are nearly the same, even though a large number of potential wells were sampled by the electrons. This finding is consistent with the descriptive model of electron motion presented in Sec. II.

### C. Radial profile of ionizations

A useful quantity that can be obtained from  $\rho_i(r, z)$  is the radial ionization profile,

$$n_r(r) = \frac{1}{2\pi r} \int \rho_i(r, z) dz \quad (4)$$

which represents the number of ionizations per unit area above the cathode. Recall that in our model, the ions fall directly down to the cathode from the ionization site without radial deflection. Therefore,  $n_r(r)$  can be directly compared to experimental measurements of the radial profile of the ion flux striking the cathode.

This ion flux is easy to measure. One indication is the depth of the etch track in the cathode material. After a number of hours of operating our planar magnetron in argon, we measured the etch track profile in the copper cathode.<sup>7</sup> It had a maximum depth of 2 mm. In Fig. 8 a plot of this experimentally obtained profile is overlaid on a plot of the radial ionization distribution computed from our Monte Carlo results. The agreement between the model and the experimental data is good.

This comparison is successful despite the fact that the etch track was formed by operating the magnetron at a number of

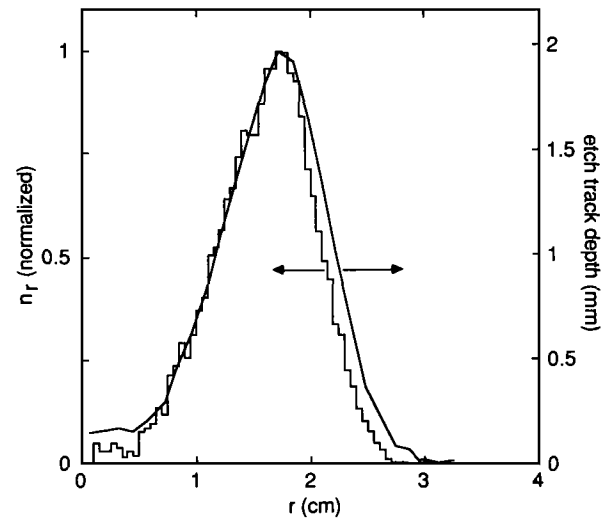


FIG. 8. Radial profile of ionizing collisions,  $n_r(r)$ , from the simulation, compared to etch track depth from experimental measurements. The vertical scales for the two curves were adjusted to make the heights of their peaks match. The agreement is good.

different pressures and cathode biases. (Better experimental data could be obtained in the fashion of Wendt *et al.* by imbedding current probes in the magnetron cathode surface.<sup>5</sup>)

Our finding that the shape of the etch track can be predicted accurately lends confidence to the model.

### D. Axial profile of ionizing collisions

Inelastic collisions produce the optical emission from a magnetron discharge. For most atomic gases, the visible light that an observer can see originates from transitions between the excited states. Consequently, the optical emission from a magnetron can be modeled by recording the locations of the inelastic collisions that result in exciting the neutral to a highly excited state.

As a proxy for excitations to those highly excited states, here we will use the ionization events. This is a suitable approximation because the total ionization and excitation cross sections have nearly the same dependence on electron energy.

The axial distribution of ionizing collisions  $n_z(z)$  was computed by integrating the ionization density radially and is shown in Fig. 9. Note the appearance in this illustration of a cathode dark space between  $0 < z < 2$  mm. There is also a peak in  $n_z(z)$  at  $z = 3$  mm.

This figure can be compared to an experimental measurement of axial distribution of optical emission, which will also display a dark space as well as a peak in the emission a few millimeters from the cathode. Such a measurement was reported by Gu and Lieberman.<sup>17</sup> They used an optical apparatus that had an axial spatial resolution of 0.28 mm to detect the total visible emission along a radial chord. Their experiment is suited for a test of our numerical results shown in Fig. 9, although the comparison can only be qualitative because we used a different magnetic configuration. We do find qualitative agreement between our simulation and their experiment.

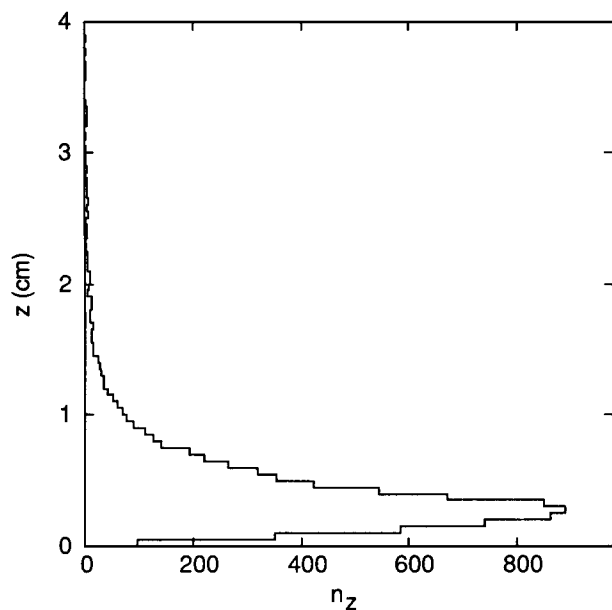


FIG. 9. Axial profile of ionizing collisions from the model,  $n_z(z)$ . The cathode is located at  $z = 0$ . This can be compared to experimental measurements of the axial optical emission profile, such as the one reported in Ref. 17. Note the appearance of a cathode dark space for  $0 < z < 2$  mm.

## VI. CONCLUSIONS

We have presented a model of energetic electron transport in magnetron plasmas. This single particle description is applicable to all magnetron geometries. We have reduced the problem by making a number of approximations. Most notably, we allow scattering of electrons by only three types of collisions (ionization, excitation, and elastic scattering), and we track single electron orbits in prescribed magnetic and electric fields.

We have applied the model by developing a Monte Carlo orbit code. For the present purposes, we used it to gain an understanding of the physical processes involved in magnetron discharges, although it may also be practical for designing optimum magnetron configurations.

As a test of the Monte Carlo method, we simulated the electrons emitted from the cathode of a planar magnetron. A two-dimensional  $B$  field and a one-dimensional  $E$  field were assumed. We found that cathode emission results in an aver-

age of 14.26 ionizations per electron for a 400 V discharge in argon at a pressure of 1 Pa. This high efficiency of ionization is attributable to the electron confinement brought about by the magnetron's effective potential well and by the predominance of forward scattering. The spatial distribution of ionization predicted in the simulation was compared to experimental measurements of the radial ion current profile and the axial optical emission profile. These tests show good agreement between theory and experiment, indicating that the model can accurately characterize the locations in the discharge where ionization takes place.

## ACKNOWLEDGMENTS

The authors thank Mark Kushner and Amy Wendt for helpful discussions. This work was funded by a grant from the Iowa Department of Economic Development and an IBM Faculty Development Award.

<sup>1</sup>John A. Thornton and Alan S. Penfold, in *Thin Film Processes*, edited by J. L. Vossen and W. Kern (Academic, New York, 1978), p. 75.

<sup>2</sup>Robert K. Waits, in Ref. 1, p. 131.

<sup>3</sup>David B. Fraser, in Ref. 1, p. 115.

<sup>4</sup>Francis F. Chen, *Introduction to Plasma Physics and Controlled Fusion*, 2nd ed. (Plenum, New York, 1984), p. 190.

<sup>5</sup>A. E. Wendt, M. A. Lieberman, and H. Meuth, *J. Vac. Sci. Technol. A* **6**, 1827 (1988), and A. E. Wendt, Ph.D. thesis, University of California at Berkeley, 1988.

<sup>6</sup>S. M. Rossnagel and H. R. Kaufman, *J. Vac. Sci. Technol. A* **6**, 223 (1988).

<sup>7</sup>T. E. Sheridan and J. Goree, *J. Vac. Sci. Technol. A* **7**, 1014 (1989).

<sup>8</sup>George Schmidt, *Physics of High Temperature Plasmas*, 2nd ed. (Academic, New York, 1979), Secs. 2-6.

<sup>9</sup>T. E. Sheridan and J. Goree, U. of Iowa Report No. 89-13, *IEEE Trans. Plasma Sci.* (in press).

<sup>10</sup>C. E. Roberts, *Ordinary Differential Equations: A Computational Approach* (Prentice-Hall, Englewood Cliffs, NJ, 1979).

<sup>11</sup>David B. Medved and Y. E. Strausser, *Adv. Electronics Electron Phys.* **21**, 101 (1965).

<sup>12</sup>R. J. Carman, *J. Phys. D* **22**, 55 (1989).

<sup>13</sup>E. W. McDaniel, *Collision Phenomena in Ionized Gases* (Wiley, New York, 1964).

<sup>14</sup>Makoto Hayashi, Nagoya Institute of Technology Report No. IPPJ-AM-19, Research Information Center, IPP/Nagoya University, Nagoya, Japan, 1981, errata 1982.

<sup>15</sup>F. J. deHeer, R. H. J. Jansen, and W. van der Kaay, *J. Phys. B* **12**, 979 (1979).

<sup>16</sup>S. N. Nahar and J. M. Wadehra, *Phys. Rev. A* **35**, 2051 (1987).

<sup>17</sup>Lan Gu and M. A. Lieberman, *J. Vac. Sci. Technol. A* **6**, 2960 (1988).